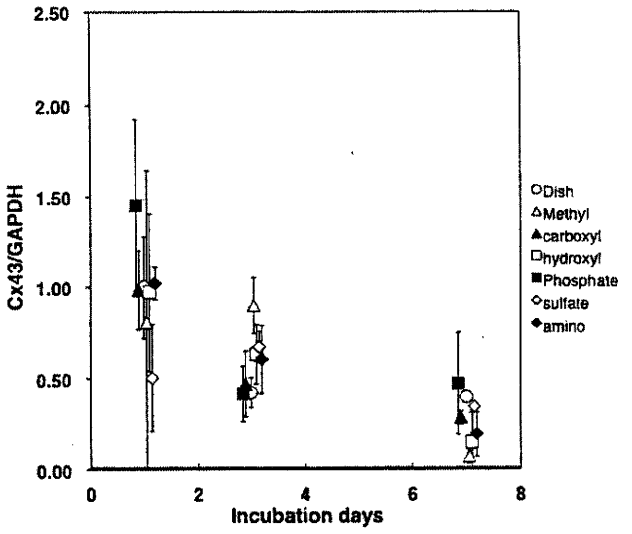

FIGURE 4. Expression levels of connexin 43 mRNA in NHOsts cultured on various SAM surfaces ($n = 3$). The expression levels of the connexin 43 mRNA were normalized by GAPDH mRNA expression level estimated from the same samples of total RNA and expressed as a ratio against the expression level in NHOsts on a collagen-coated culture dish after 1-day culture. NHOsts were cultured on a collagen-coated dish (open circle), SAM-CH_3 (open triangle), SAM-COOH (closed triangle), SAM-OH (open square), SAM-OPO_3H_2 (closed square), SAM-OSO_3H (open diamond), and SAM-NH_2 (closed diamond).

independent of their GJIC function. It was also expected that GJIC of NHOsts on SAM-CH_3 would be different from others since less NHOst proliferation on the SAM suggested a possible perturbation in homeostasis of the NHOsts. Decrease in the cell number on the SAM after 1-week incubation, however, made GJIC measurement unable because few cells contacting with two other neighboring cells were found. On the other hand, the GJIC after 1-week culture did not show any statistical differences between NHOsts on other tested SAM surfaces and those on a collagen-coated culture dish (data not shown). In addition, Figure 4 has revealed that surface functional groups of SAM do not affect mRNA expression level of connexin 43 during 1-week culture, indicating that the functional group do not affect signal cascades of connexin 43 expression in NHOsts. To study effects of the functional group as well as hydrophilic/hydrophobic balance of the surface on GJIC more in detail, changes in GJIC level of cells on the surfaces are under investigation utilizing metabolic cooperation assay system. Results of the study will be reported in near future. However, this study suggests that an enhancement of differentiation level of NHOsts induced by phosphorylated or sulfate group on the surface is triggered by a direct interaction between the chemical group and NHOsts, followed by signal cascades in which GJIC does not participate. In fact, sulfated polysaccharides have been reported to affect expression of several genes relating to cell differentiation,[15] but a mechanism of the sulfated group to affect the expression of these genes remains to be clarified. The details of the interaction and the signal cascades will be clarified in future studies.

CONCLUSIONS

This study suggests that the functional groups covering surface have the potential to control attachment, proliferation, and differentiation of NHOsts cultured on it. Figures of NHOsts after 1-day culture and the cell numbers estimated after 1-week culture indicate that hydrophilic/Hydrophobic balance of the surfaces may be one of key factors to regulate attachment and proliferation of NHOsts on the surfaces. Although the proliferation level decreased, the surface covered with either phosphate or sulfate group showed an enhancement in differentiation level of cultured NHOsts through unidentified signal cascades triggered by these functional groups and independent of GJIC. This suggests that ionic charge level of the functional groups is one of key factors to regulate osteogenic differentiation on the surfaces more than hydrophilic/hydrophobic balance of the surfaces. Further studies are necessary for clarifying the mechanisms of different differentiation levels of NHOsts induced by interaction with the functional groups as well as for future applications of SAMs in the fields of medical devices and tissue engineering.

ACKNOWLEDGMENTS

Authors are grateful to Professor Toshiaki Enoki and Associate Professor Ken-ichi Fukui (currently Professor of Osaka University), Tokyo Institute Technology for their kind permission to utilize electron-beam evaporation equipment for chromium precoating. Authors are also grateful to Dr. Rumi Sawada, Division of Medical Devices, NIHS, Japan, for her kind support in real-time PCR experiments.

REFERENCES

1. Adams JC, Watt FM. Regulation of development and differentiation by the extracellular matrix. Development 1993;117:1183–1198.
2. Peterson WJ, Tachiki KH, Yamaguchi DT. Extracellular matrix alters the relationship between thymidine incorporation and proliferation of MC3T3-E1 cells during osteogenesis *in vitro*. Cell Prolif 2002;35:9–22.
3. Hirano Y, Okuno M, Hayashi T, Goto K Nakajima A. Cell-attachment activities of surface immobilized oligopeptides RGD, RGDS, RGDV, RGDT, and YIGSR toward five cell lines. J Biomater Sci Polym Ed 1993;4:235–243.
4. Alsberg E, Anderson KW, Albeiruti A, Rowley JA, Mooney DJ. Engineering growing tissues. Proc Natl Acad Sci 2002;99: 12025–12030.
5. Bisson I, Kosinski M, Ruault S, Gupta B, Hilborn J, Wurm F, Frey P. Acrylic acid grafting and collagen immobilization on poly(ethylene terephthalate) surfaces for adherence and growth of human bladder smooth muscle cells. Biomaterials 2002;23:3149–3158.
6. Nakaoka R, Tsuchiya T. Neural differentiation of midbrain cells on various protein-immobilized polyethylene films. J Biomed Mater Res A 2003;64:439–446.
7. Masters KS, Shah DN, Walker G, Leinwand LA, Anseth KS. Designing scaffolds for valvular interstitial cells: Cell adhesion and function on naturally derived materials. J Biomed Mater Res A 2004;71:172–180.
8. Kong HJ, Boontheekul T, Mooney DJ. Quantifying the relation between adhesion ligand-receptor bond formation and cell phenotype. Proc Natl Acad Sci 2006;103:18534–18539.
9. Wilson CJ, Clegg RE, Leavesley DI, Pearcy MJ. Mediation of biomaterials-cell interactions by adsorbed proteins: A review. Tissue Eng 2005;11:1–18.
10. Ulman A. Formation and structure of self-assembled monolayers. Chem Rev 1996;96:1533–1554.

11. Mrksich M, Whitesides GM. Using self-assembled monolayers to understand the interactions of man-made surfaces with proteins and cells. Annu Rev Biophys Biomol Struct 1996;25:55–78.
12. Senaratne W, Andruzzi L, Ober CK. Self-assembled monolayers and polymer brushes in biotechnology: Current applications and future perspectives. Biomacromol 2005;6:2427–2448.
13. Fujimoto H, Yoshizako S, Kato K, Iwata H. Fabrication of cell-based arrays using micropatterned alkanethiol monolayers for the parallel silencing of specific genes by small interfering RNA. Bioconjugate Chem 2006;17:1404–1410.
14. Shin SK, Yoon HJ, Jung YJ, Park JW. Nanoscale controlled self-assembled monolayers and quantum dots. Curr Opin Chem Biol 2006;10:423–429.
15. Nagira T, Nagahata-Ishiguro M, Tsuchiya T. Effect of sulfated hyaluronan on keratinocyte differentiation and Wnt and Notch gene expression. Biomaterials 2007;28:844–850.
16. Maio AD, Vaga VL, Contreras JE. Gap junctions, homeostasis, and injury. J Cell Physiol 2002;191:269–282.
17. Tsuchiya T, Hata H, Nakamura A. Studies on the tumor-promoting activity of biomaterials: Inhibition of metabolic cooperation by polyetherurethane and silicone. J Biomed Mater Res 1995;29: 113–119.
18. Tsuchiya T, Takahara A, Cooper SL, Nakamura A. Studies on the tumor-promoting activity of polyurethanes: Depletion of inhibitory action of metabolic cooperation on the surface of a polyalkyleneurethane but not a polyetherurethane. J Biomed Mater Res 1995;29:835–841.
19. Nakaoka R. Tsuchiya T, Sakaguchi K, Nakamura A. Studies on *in vitro* evaluation for the biocompatibility of various biomaterials: Inhibitory activity of various kinds of polymer microspheres on metabolic cooperation. J Biomed Mater Res 2001;57:279–284.
20. Nakaoka R, Tsuchiya T, Nakamura A. The inhibitory mechanism of gap junctional intercellular communication induced by polyethylene and the restorative effects by surface modification with various proteins. J Biomed Mater Res 2001;57:567–574.
21. Nagahata M, Nakaoka R, Teramoto A, Abe K, Tsuchiya T. The responses of normal human osteoblasts to anionic polysaccharide polyelectrolyte complexes. Biomaterials 2005;26:5138–5144.
22. Nakaoka R, Tsuchiya T. Enhancement of differentiation and homeostasis of human osteoblasts by interaction with hydroxyapatite in microsphere form. Key Eng Mater 2006;309–311:1293–1298.
23. Tanahashi M, Matsuda T. Surface functional group dependence on apatite formation on self-assembled monolayers in a simulated body fluid. J Biomed Mater Res 1997;34:305–315.
24. Hamano T, Chiba D, Nakatsuka K, Nagahata M, Teramoto A, Kondo Y, Hachimori A, Abe K. Evaluation of a polyelectrolyte complex (PEC) composed of chitin derivatives and chitosan, which promotes the rat calvarial osteoblast differentiation. Polym Adv Technol 2002;13:46–53.
25. Ohyama M, Suzuki N, Yamaguchi Y, Maeno M, Otsuka K, Ito K. Effect of enamel matrix derivative on the differentiation of C2C12 cells. J Periodontol 2002;73:543–550.
26. Wade MH, Trosko JE, Schlindler M. A fluorescence photobleaching assay of gap junctional-mediated communication between human cells. Science 1986;232:525–528.
27. Ito Y. Surface micropatterning to regulate cell functions. Biomaterials 1999;20:2333–2342.
28. Hamilton DW, Brunette DM. The effect of substratum topography on osteoblast adhesion mediated signal transduction and phosphorylation. Biomaterials 2007;28:1806–1819.
29. Bertilsson L, Liedberg B. Infrared study of thiol monolayer assemblies on gold: Preparation, characterization, and functionalization of mixed monolayers. Langmuir 1993;9:141–149.
30. Mrksich M, Chen CS, Xia Y, Dike LE, Ingber DE, Whitesides GM. Controlling cell attachment on contoured surfaces with self-assembled monolayers of alkanethiolates on gold. Proc Natl Acad Sci 1996;93:10775–10778.
31. McClary KB, Ugarova T, Grainger DW. Modulating fibroblast adhesion, spreading, and proliferation using self-assembled monolayer films of alkylthiolates on gold. J Biomed Mater Res 2000;50: 428–439.
32. Scotchford CA, Gilmore CP, Cooper E, Leggett GJ, Downes S. Protein adsorption and human osteoblasts-like cell attachment and growth on alkylthiol on gold self-assembled monolayers. J Biomed Mater Res A 2002;59:84–99.
33. Cox JD, Curry MS, Skirboll SK, Gourley PL, Sasaki DY. Surface passivation of a microfluidic device to glial cell adhesion: A comparison of hydrophobic and hydrophilic SAM coatings. Biomaterials 2002;22:929–935.
34. Howlett CR, Evans MDM, Walsh WR, Johnson G, Steele JG. Mechanism of initial attachment of cells derived from human bone to commonly used prosthetic materials during cell culture. Biomaterials 1994;15:213–222.
35. Kilpadi KL, Chang PL, Bellis SL. Hydroxyapatite binds more serum proteins, purified integrins, and osteoblast precursor cells than titanium or steel. J Biomed Mater Res A 2001;57:258–267.
36. Kidoaki S, Matsuda T. Mechanistic aspects of protein/material interactions probed by atomic force microscopy. Colloids Surf B 2002;23:153–163.
37. Lecanda F, Towler DA, Ziambaras K, Cheng SL, Koval M, Steinberg TH, Civitelli R. Gap junctional communication modulates gene expression in osteoblastic cells. Mol Biol Cell 1998;9: 2249–2258.
38. Donahue HJ, Li Z, Zhou Z, Yellowley CE. Differentiation of human fetal osteoblastic cells and gap junctional intercellular communication. Am J Physiol Cell Physiol 2000;278:C315–C322.

///VSP///

Journal of Biomaterials Science 21 (2010) 1957–1970

Journal of BIOMATERIALS SCIENCE
brill.nl/jbs

Self-Organization of the Compositional Gradient Structure in Hyaluronic Acid and Poly(N-isopropylacrylamide) Blend Film

Bayar Hexig [a,*], Kazuo Isama [b], Yuji Haishima [b], Yoshio Inoue [a], Toshie Tsuchiya [b,c] and Toshihiro Akaike [a,d]

[a] Department of Biomolecular Engineering Graduate School of Bioscience and Biotechnology, Tokyo Institute of Technology, 4259 Nagatsuta-cho, Midori-ku, Yokohama-shi 222-8501, Japan

[b] Division of Medical Devices, National Institute of Health Sciences, Kamiyoga, 1-18-1 Setagaya-ku, Tokyo 158-8501, Japan

[c] Medical center for Translational Research, Osaka University Hospital, 2-15 Yamadaoka, Suita, Osaka 565-0871, Japan

[d] Frontier Research Center, Tokyo Institute of Technology, 4259 Nagatsuta-cho, Midori-ku, Yokohama-shi 222-8501, Japan

Received 13 May 2010; accepted 23 August 2010

Abstract

A compositional gradient structure in hyaluronic acid (HA) and poly(N-isopropylacrylamide) (PIPAAm) blend film was self-organized from a homogeneous aqueous solution in a plasma-treated polystyrene dish (PTPSD), and the formation mechanisms of the gradient structure were studied by casting the same solution on PTPSD and a non-treated polystyrene dish (NTPSD) under ambient and vacuum conditions. The formation of a compositional gradient structure in HA/PIPAAm blend film was confirmed by scanning electron microscopy, energy dispersive X-ray (EDX) mapping analysis and step-scan photoacoustic Fourier transformed infrared spectroscopy (PAS–FT-IR) measurements. The EDX mapping measurements for Na element revealed that the HA component gradually decreases from the dish-side to the air-side of the film cast on PTPSD, while for the film cast on NTPSD no such obvious change was observed on the cross-section. Further studies on the films prepared on PTPSD and NPTPSD under ambient and vacuum conditions demonstrated that the hydrophilic interaction and the solvent evaporation rate were the most significant factors leading to the formation of a compositional gradient structure in the HA/PIPAAm blend system.

Keywords

Self-organization, FGM, hyaluronic acid, poly(N-isopropylacrylamide)

* To whom correspondence should be addressed. E-mail: bhexig@bio.titech.ac.jp

DOI:10.1163/092050610X528589

1. Introduction

Biomimetic and bioinspired optimal structures combining bioresorbable, bioactive and other advanced properties are expected for the next generation of biomaterials [1–3]. Inspired by nature, to reveal the relationship between structure and functionality of biological materials has been emphasized in the biomaterials research field, and self-organization of a polymeric system has been recognized as a key challenge for producing functional materials that combine several properties and the inherent beauty of ordered structures [4, 5]. In nature, gradient biological structures exist most commonly, such as the structure of bamboo [6], shells, teeth, bones, tendon and extracellular matrix (ECM) [7]. Man-made functionally gradient materials (FGMs) have been developed for combining irreconcilable properties within a single material and have been widely incorporated in metal/ceramic and organic/inorganic material fields for increasing the structural complexity and combining different functionality [8–10].

Recently, there have been many efforts to develop polymeric FGMs with unique properties and advanced functions that are inaccessible in conventional uniform systems [11, 12]. Many preparation approaches have been developed to generate a polymeric functionally gradient structure during homogenization or segregation processes [13–16]. Despite these efforts made recently to generate polymeric FGMs, characterization of their gradient structure, physico-chemical properties and elucidation of formation mechanisms still remain to be explored. Previously, the spontaneous formation of a chitosan/poly(vinyl alcohol) compositional gradient structure on a aluminum dish from a homogeneous aqueous solution was reported, and the gradient film was found to show some unique physical properties compared to a homogeneous blend film which was prepared on a Teflon dish [12]. However, there is still no detailed understanding of the formation mechanisms of such a compositional gradient structure spontaneously formed on a aluminum dish. It requires both the hydrophilic and hydrophobic properties incorporated into the same material surfaces, but it is extremely difficult to control these on the metallic substrate's surface because oxidation occurs at any given moment in ambient conditions.

Plasma technology can add functional groups to a surface of organic and inorganic materials at the molecular level, changing surface chemistries to obtain increased bond strength, hydrophilicity, permeability, and activating and changing surfaces from hydrophobic to hydrophilic without affecting the bulk properties. In the present study, we show a compositional gradient structure in a HA/PIPAAm blend film self-organized during the solvent evaporation process on a oxygen-plasma treated polystyrene dish (PTPSD), while on the non-treated polystyrene dish (NTPSD) a nearly homogenous blend film was formed at ambient condition.

HA is a naturally occurring linear polysaccharide, widely distributed in the body as a component of ECM of connective tissues, and recently HA-based biomaterials have been utilized for a variety of clinical applications and tissue engineering of skin, cartilage tissue and bone, based upon its specific properties, excellent biocompatibility and bioactivity [17–21]. PIPAAm is a synthetic polymer which has a sharp

and reversible phase transition at approx. 32°C and is applicable in tissue engineering as a functional hydrogel and as a cell sheet [22, 23]. It is interesting to develop a novel biomaterial combining the biocompatibility, bioactivity of HA and the inherent thermal responsibility of PIPAAm in the tissue engineering field. For improving the biocompatibility of PIPAAm hydrogel, intensive studies have been done to develop a series of thermosensitive co-polymers by coupling carboxylic end-capped PIPAAm to HA through amide bond linkages [24–26]. In the present study, we aimed to prepare a composite material of HA and PIPAAm with a gradual change in chemical composition which combines not only the inherent properties of two components, but also those of their complex with various compositions. It is expected that such a compositional gradient material could provide rather advanced and new properties compared to the conventional composite material with a given compositional ratio of the components. A compositional gradient structure in bioactive sodium hyaluronic acid (HA) and thermal-responsive poly(N-isopropylacrylamide) (PIPAAm) blend film was simply self-organized from a homogeneous aqueous solution on a plasma-treated polystyrene dish (PTPSD) at room temperature. The formation mechanism was studied by casting the same solution on PTPSD and non-treated polystyrene dish (NTPSD) under ambient and vacuum conditions at room temperature. Our findings demonstrate that the hydrophilic interaction with substrate and the solvent evaporation rate were the most significant factors for the formation of the compositional gradient structure in the HA/PIPAAm blend system.

2. Materials and Methods

2.1. Materials

2.1.1. Film Preparation

A 1 wt% HA solution was prepared by dissolving powder HA (weight-average molecular weight 1 680 000 by GPC, Life Core Biomedical) in distilled water with stirring for 24 h. A 1 wt% PIPAAM solution was prepared by diluting 15 wt% PIPAAm (weight-average molecular weight 220 000 by GPC, Kohjin) aqueous solution with distilled water with stirring for 24 h. Thereafter the 1 wt% HA and 1 wt% PIPAAm solutions were mixed together at the same weight ratio and stirred further for 24 h before casting on PTPSD and NTPSD in ambient and vacuum conditions. For the preparation of films from the same amount of solution with the same concentration, it needed 48 h in ambient conditions, while it needed only 12 h in vacuum. All resulting films were heated at 80°C under vacuum condition for 5 h before evaporation of the remained water in the film and characterization.

2.2. Plasma Treatment of the Polystyrene Dish

The plasma treatment was performed with a SWP-101EX (Nissin), using low-pressure region output power of the microwave oscillator at 2.0 kW; the polystyrene dishes were set on the sample stage which is 15 cm below the reactor. The oxygen

discharge was utilized and the oxygen was filled at a rate of 500 cc/min at a pressure of 70 Pa. Plasma irradiation was performed for 15 s.

2.3. X-Ray Photoelectron Spectroscopy (XPS)

The XPS analyses were performed with an ESCA-3200 spectrometer (Shimadzu), using a magnesium Kα X-ray source (1253.6 eV). The high-resolution spectra of the C_{1s}, O_{1s} and Na_{1s} regions were recorded with a pass energy of 75 eV at 45° take-off angle.

2.4. Scanning Electron Microscopy (SEM) and Energy Dispersive X-Ray (EDX) Analysis

A JSM-5800LV (JEOL) equipped with an EX-23000BU EDX detector was used to analyze the freeze-fractured cross-section geometry, the chemical composition and element mapping measurements. The samples were fractured at liquid-nitrogen temperature, and sputtered with gold before taking micrographs.

2.5. Step-Scan Photoacoustic Fourier Transformed Infrared Spectroscopy (PAS–FT-IR)

PAS–FT-IR spectra measurements were carried out on a JIR-SPX200 FT-IR spectrometer (JEOL) equipped with a MTEC 300 photoacoustic cell (MTEC Photoacoustic). Prior to the start of the penetration experiment the cell was purged with helium for 30 s.

3. Results and Discussion

3.1. Surface Analysis of the Compositional Gradient Film

Figure 1 shows the molecular structures and XPS spectra of pure PIPAAm, pure HA, and the difference of chemical compositions between two surfaces of the blend film cast from homogeneous aqueous solution with the same compositional fraction of HA/PIPAAm (50%/50%) on PTPSD at room temperature, and the C_{1s} and Na_{1s} core level regions are also shown. For pure PIPAAm, the C_{1s} spectrum is decomposed by peak fitting to two components at 285.0 and 287.9 eV, corresponding to the hydrocarbon (*HC*) (including carbon singly bound to nitrogen (*CN*)) and the carbon atom in carbonyl group environments, respectively. The high-resolution C_{1s} spectrum of HA is decomposed to four peaks at 285.0 ± 0.1, 286.6 ± 0.1, 288.1 ± 0.1 and 289.5 ± 0.1 eV, corresponding to the *HC* (including *CN*), carbon singly bound to oxygen (*CO*), carbon doubly bonded to oxygen (*OCO*) (including amide and carboxylate ion carbon atoms (*CON* and *COO*)), and finally carbon in an ester environment (COOR), respectively, resulting in a very close match to the experimentally observed spectrum. Both the high-resolution XPS spectra in C_{1s} and Na_{1s} core level regions were obviously different between two surfaces of the HA/PIPAAm film cast on PTPSD at room temperature. The spectra of the air-side surface are close to that of pure PIPAAm (Fig. 1c) and the spectra of the dish-side surface are close to that

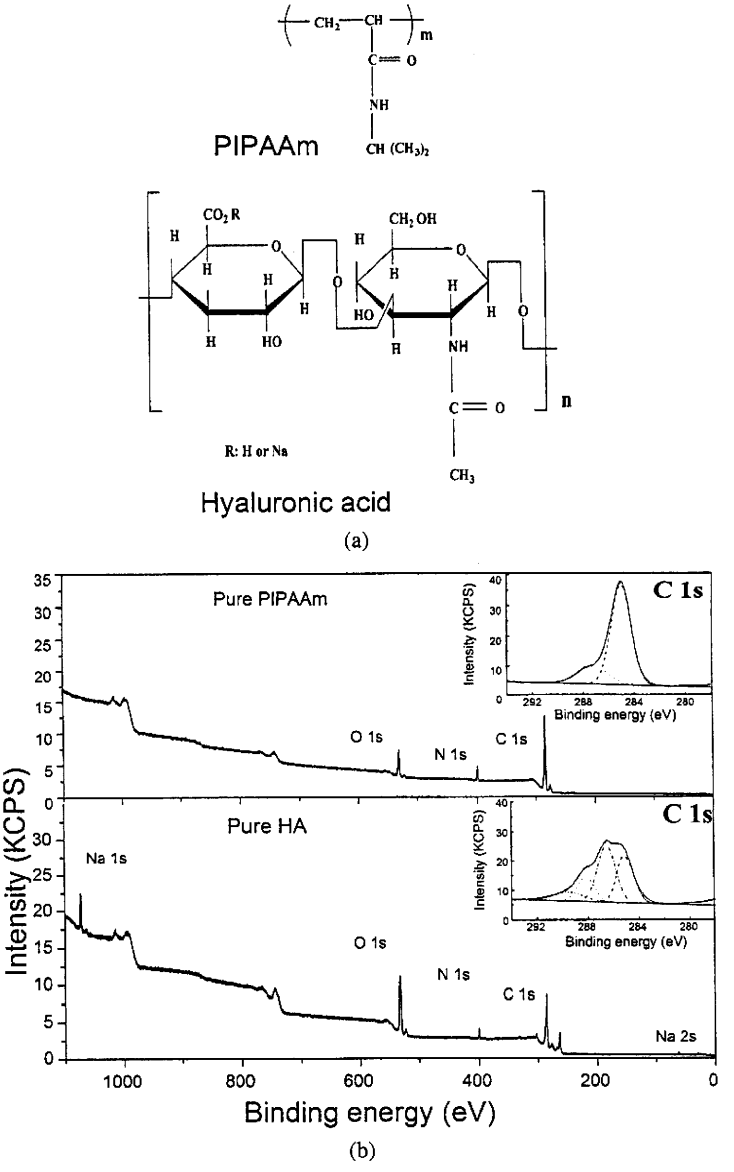

Figure 1. (a) Molecular structure of pure PIPAAm and pure HA. (b) XPS spectra of pure PINPAAm and pure HA. The inset shows the corresponding magnification of the C_{1s} core level regions and the results resolved by the curve-fitting program. Dashed line, HC; dash-dotted line, CO; dotted line, OCO; dash-dot-dotted line, CON or COO; short dashed line, baseline; short dash-dotted line, curve-fitted results; solid line, experimental results. (c, d) XPS spectra of the air-side and dish-side surfaces of the film cast on PTPSD in ambient conditions, respectively. The insets are the corresponding Na_{1s} core level regions.

of pure HA (Fig. 1d). It implies that the cross-section of the film may form a gradient structure in the HA/PIPAAm blend composition along the thickness direction.

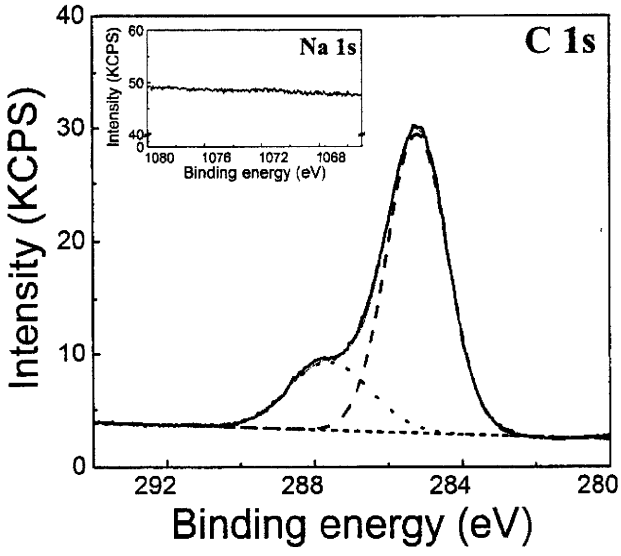

(c)

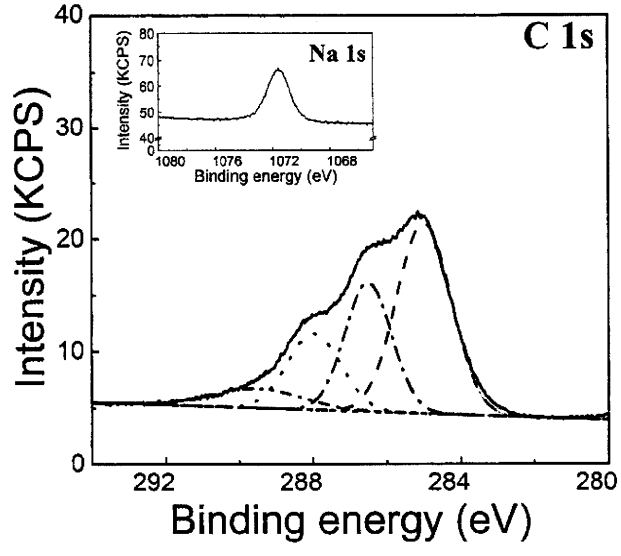

(d)

Figure 1. (Continued.)

However, no significant difference was observed in the XPS spectra of the two surfaces of HA/PIPAAm film cast on NTPSD.

3.2. Characterization of Gradient Structure of Films

The cross-section morphology and distribution of chemical composition along the thickness direction were investigated by means of SEM and EDX analysis, respectively. Figure 2 shows the EDX spectra of pure HA, pure PIPAAm, SEM

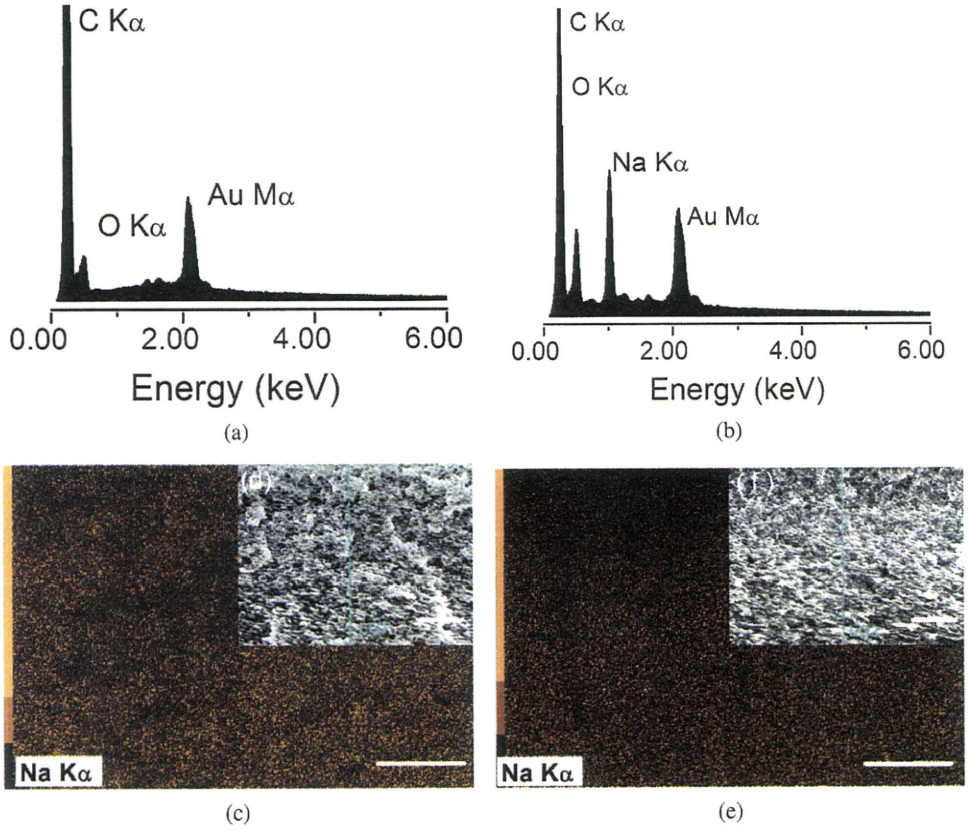

Figure 2. (a) EDX spectrum of pure PIPAAm film. (b) EDX spectrum of pure HA film. (c) EDX mapping measurements for Na on a freeze-fractured cross-section of the film cast on NTPSD. The inset (d) is the corresponding SEM image. (e) EDX mapping measurements for Na on a freeze-fractured cross-section of the film cast on PTPSD. The inset (f) is the corresponding SEM image. Scale bar = 100 μm. This figure is published in colour in the online edition of this journal, that can be accessed *via* http://www.brill.nl/jbs

micrographs of the cross-sections and EDX mapping measurements of Na for the two films cast on NTPSD and PTPSD. In Fig. 2 light areas correspond to a high concentration of Na atoms, and dark areas to a low concentration. It is clearly observed that the distribution of Na atoms, which is a probe element of HA, gradually changes along the thickness direction of the film cast on PTPSD, while no significant changes were observed for the film cast on NTPSD in ambient conditions. The results of EDX mapping for Na atoms strongly indicate that the composition of HA and PIPAAm gradually changes along the film thickness direction.

3.3. Surface Analyses of NTPSD, PTPSD and Formation of Gradient Structure

As shown in Fig. 3a and 3b, the characteristic surface property of PTPSD is much more hydrophilic due to the added functionally oxidized groups on the surface by oxygen plasma treatment. The mechanism of spontaneous formation of the compo-

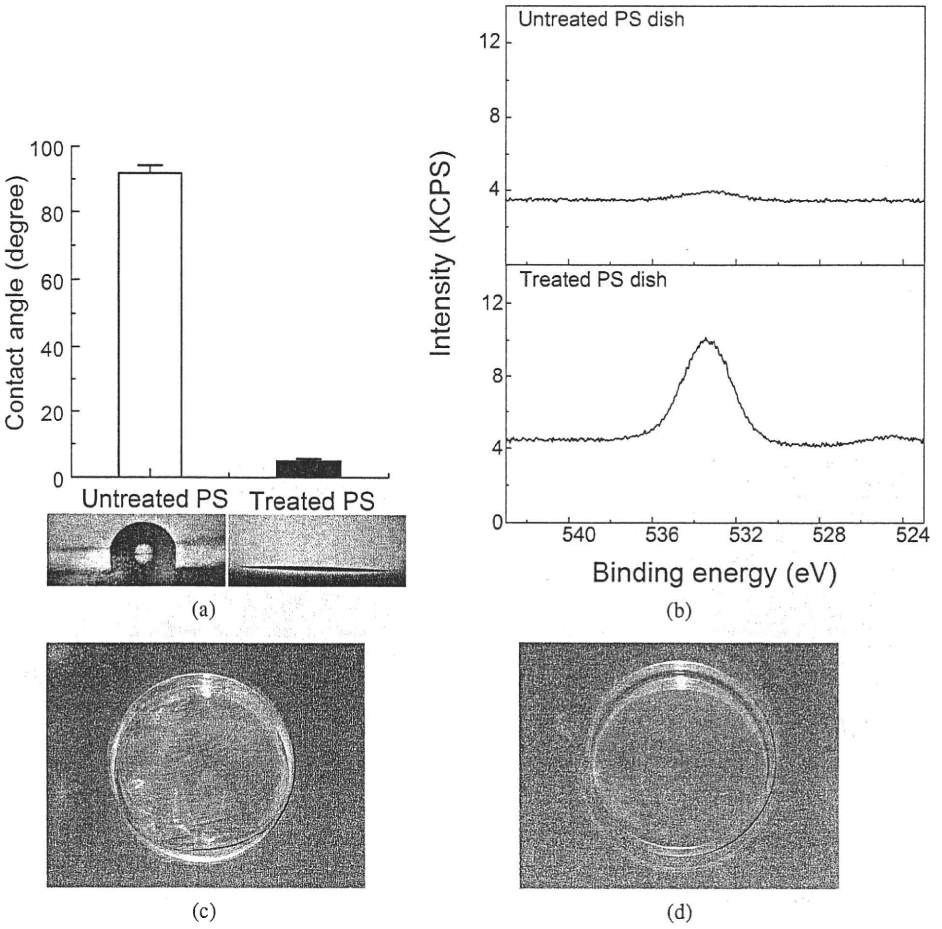

Figure 3. (a) Hydrophilicity measured by the contact angle of a water drop with NTPSD and PTPSD. Representative images are shown below. (b) XPS spectra in the O_{1s} core level region of the NTPSD and PTPSD surfaces. (c, d) The resulting film cast on NTPSD and PTPSD in vacuum conditions, respectively.

sitional gradient structure in PIPAAm/HA blend film on PTPSD was further studied by casting the film in vacuum condition. As shown in Fig. 3c and 3d, the film formed on NTPSD in vacuum is detached from the dish, while the film formed on PTPSD in vacuum is adhered on the dish. Both the high-resolution C_{1s} and Na_{1s} XPS spectra of the two surfaces of the film cast on NTPSD in vacuum conditions are also different from each other, but only show HA/PIPAAm blends with different compositional fractions (Fig. 4a and 4c). The air-side surface is a HA/PIPAAm blend rich in PIPAAm, and the dish-side surface is a HA/PIPAAm blend rich in HA. However, for the film cast on PTPSD in vacuum, the air-side surface shows completely the same XPS spectra as those of PIPAAm, and the dish-side surface shows XPS spectra extremely close to those of HA (Fig. 4b and 4d).

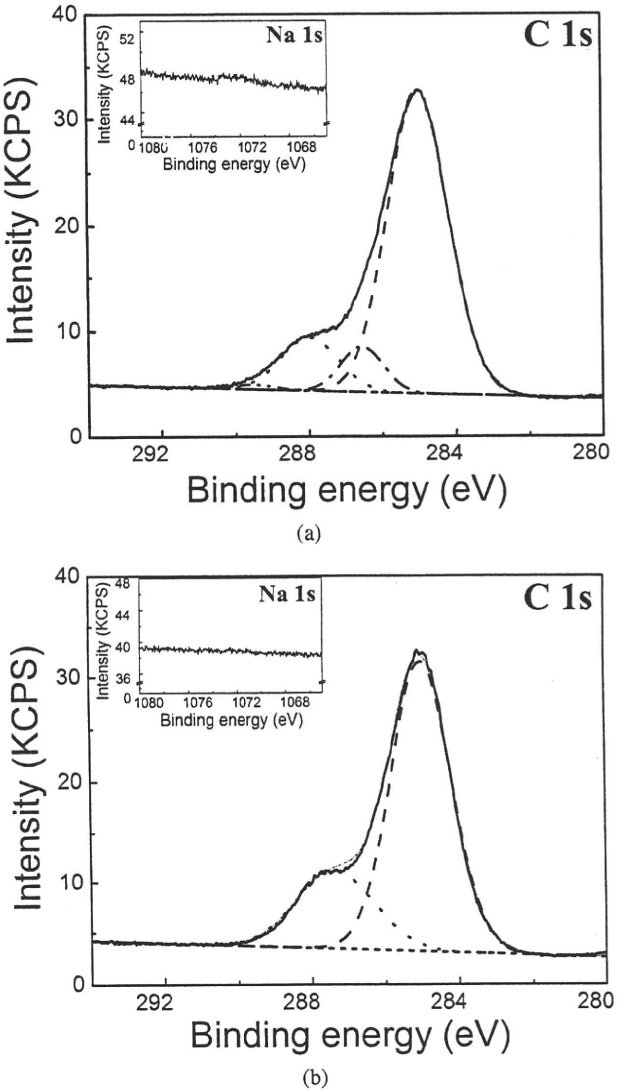

Figure 4. (a, c) XPS spectra of the C_{1s} core level region of the air-side and dish-side surfaces of the film cast on NTPSD in vacuum conditions, respectively. The insets are the corresponding Na_{1s} core level regions. (b, d) XPS spectra if the C_{1s} core level region of the air-side and dish-side surfaces of the film prepared on PTPSD in vacuum conditions, respectively. The insets are the corresponding Na_{1s} core level regions.

The characterization of the compositional distribution along the thickness direction of HA/PIPAAm films prepared under vacuum conditions on NTPSD and PTPSD was performed by means of step-scan PAS–FT-IR, SEM and EDX mapping measurement (Fig. 5). The step-scan PAS–FT-IR is a non-destructive, non-contact method with controllable sampling depth and needs little or no sample prepara-

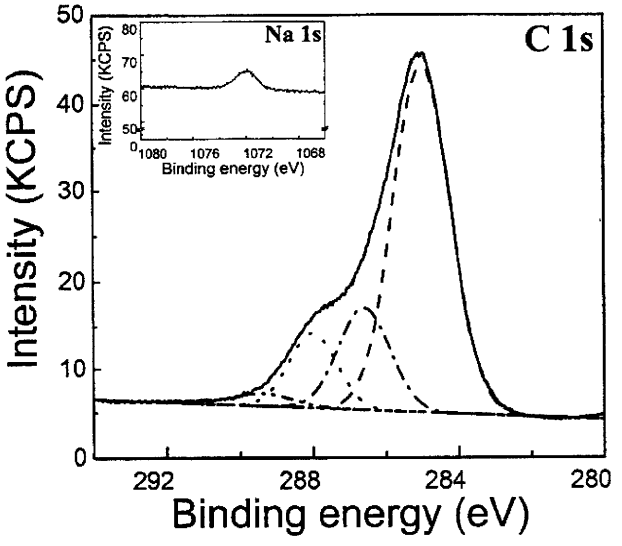

(c)

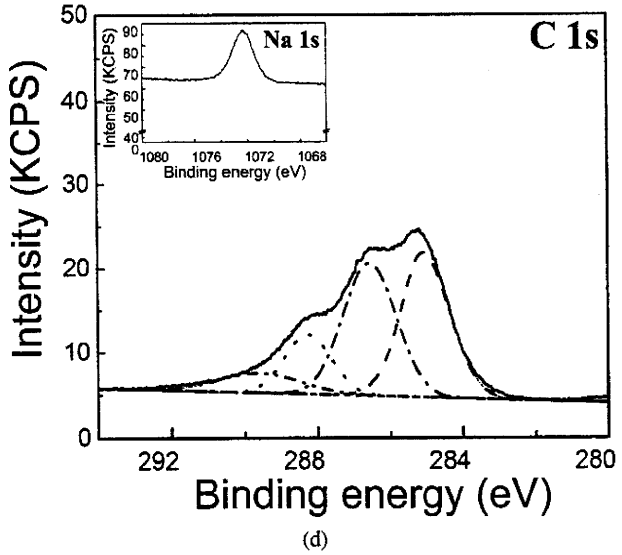

(d)

Figure 4. (Continued.)

tion. The results of PAS–FT-IR spectroscopy of increasing shallow-sampling depth corresponding to different mirror velocities of 1.0, 2.0 and 5.0 mm/s indicate that the fractions of HA and PIPAAm gradually change from the surfaces to the inside of the film for both films cast on NTPSD and PTPSD (Fig. 5a and 5b). The EDX mapping measurements for Na reveal that the HA fraction gradually decreases from the dish-side to the air-side of the film cast on PTPSD, while for the film cast on NTPSD, no such obvious change was observed on the cross-section. In order to

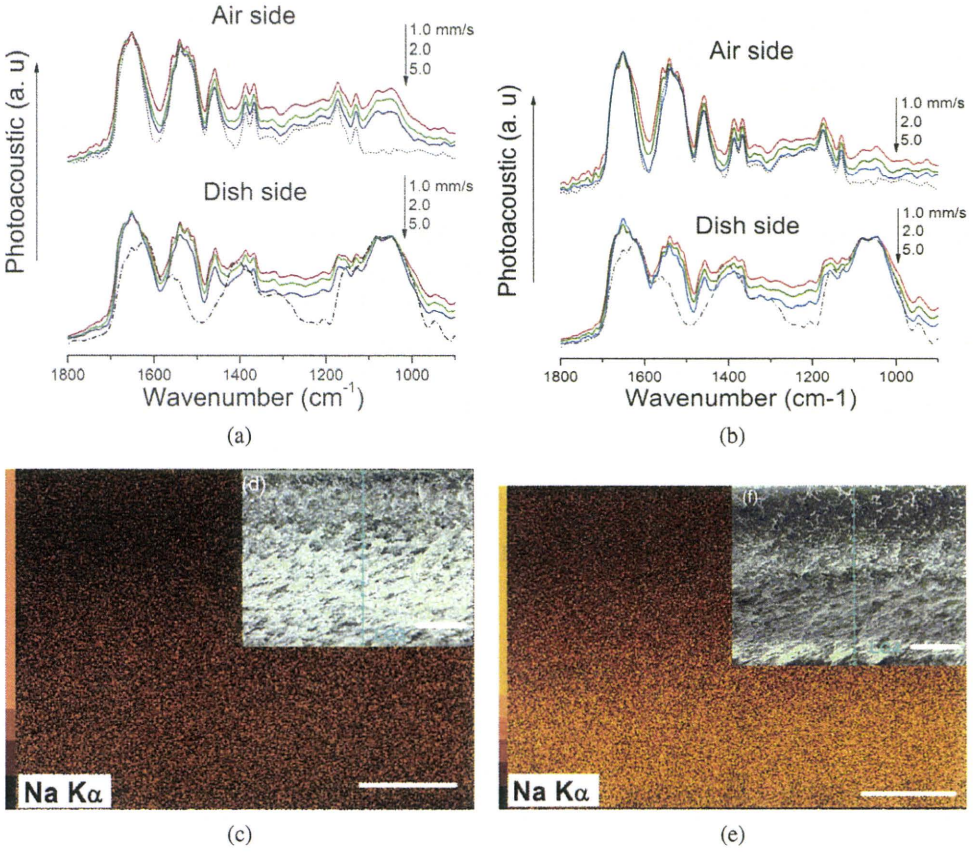

Figure 5. (a, b) PAS–FT-IR spectra with increasing shallow-sampling depth corresponding to mirror velocities of 1.0, 2.0 and 5.0 mm/s from the two surfaces of the films cast on NTPSD and PTPSD in vacuum conditions, respectively. The dotted and dash-dotted line correspond to the PAS–FT-IR spectra of pure PIPAAm and pure HA, respectively. (c, d) EDX mapping for Na and SEM image of the cross-section of the film cast on NTPSD in vacuum. (e, f) EDX mapping for Na and SEM image of the cross-section of the film cast on PTPSD in vacuum. Scale bar = 100 μm. This figure is published in colour in the online edition of this journal, that can be accessed *via* http://www.brill.nl/jbs

elucidate the contribution of the oxidized hydrophilic surface and acceleration of water molecules evaporation rate for the formation of compositional gradient structure in the HA/PIPAAm blend system, the degree of graduation of films has been plotted for mass content distribution of Na element along the thickness direction in different preparation conditions, ambient and vacuum conditions, on PTPSD and NTPSD, respectively. It is indicated that both the oxidized hydrophilic surface and evaporation rate of water molecules contribute to the formation of an ideal gradient structure in the HA/PIPAAm blend system (Fig. 6).

The formation mechanism of the compositional gradient structure in HA and PIPAAm blend system is a complicated process, related to the solubility parameters of two components, water-mediated and intermolecular hydrogen bonding network in

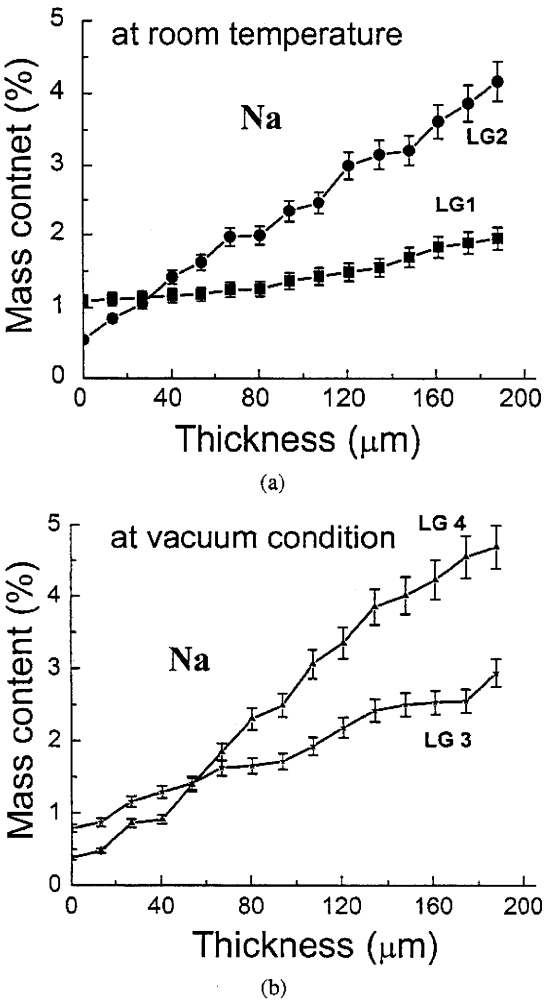

Figure 6. (a) EDX line scan results of Na on the cross-sections of films prepared in ambient conditions (LG1 for the film cast on NTPSD and LG2 for the film cast on PTPSD), (b) EDX line scan results of Na on the cross-sections of films prepared in vacuum conditions (LG3 for the film cast on NTPSD and LG4 for the film cast on PTPSD).

the blend system, and their rearrangement during the solvent evaporation process. In the homogeneous solution, the water-mediated or direct intermolecular hydrogen bonds between the functional groups of HA chain and oxidized functional groups on the PTPSD surface are constantly breaking and reforming at the urgings of thermal motion. However, because its intrinsic molecular structure, the PIPAAm chain hardly interacts with oxidized functional groups on the surface of PTPSD. In addition, the high solubility and mobility of PIPAAm makes it easy to accompany the evaporation of water molecules to move toward the air-side under the water molecule's plasticizing effect. In contrast, HA chains contain two kinds of links. The

glycosidic link between two rigid units consists of a single oxygen atom joining one sugar to the next, and each glucuronate unit carries a strong proton acceptor group associated with its carboxylate group. The unique molecular structure leads to the formation of a tape-like secondary structure and enables aggregation *via* specific interaction in water to form a meshwork, even at low concentrations [27, 28]. Therefore, once the intermolecular hydrogen bonding interaction was formed between carboxylate groups of HA and oxidized functional groups on the PTPSD surface, the water molecules' motion was not sufficient for breaking the interaction at high concentrations of HA during the evaporation process. Thus, HA molecules meshworks begin to overlap and aggregate on the PTPSD surface, resulting in changes of the film composition along the thickness direction and air-side and dish-side composition of the film, much the same as with pure PIPAAm and HA, respectively. However, on the hydrophobic surface of NTPSD, there is no strong interaction between the two components and the normal PS surface, such as intermolecular hydrogen bonds. Therefore, overlapping and aggregation of HA molecular meshworks occur in the whole mixture system under dominant contribution of entanglement, water-mediated and intermolecular interaction between HA and PIPAAm chains. The acceleration of the water molecular evaporation rate induces the delay of overlapping of HA molecular meshworks, resulting in the compositional difference between the two sides of the film. The fact that the resulting film on PTPSD, but not on NTPSD, is weakly adhered on the substrate indicates that the interactions between two components and oxidized surface of substrates are a significant factor for the formation of the gradient structure.

4. Conclusion

We prepared and characterized the compositional gradient structure in a HA/PIPAAm blend film. The formation mechanism of the functional gradient structure in a polysaccharide/polymer blend film self-organized from a homogeneous aqueous solution on PTPSD has been investigated by controlling the surface property of the casting substrate and the water evaporation rate. The gradient structure was confirmed by EDX mapping measurements for Na on the cross-section of the films and PAS–FT-IR analysis with increasing shallow-sampling depth from the two surfaces. The method of casting from a homogeneous aqueous solution is quite a simple way to prepare functional gradient polymeric materials. However, the mechanism involved in the formation of gradient structure is a complicated process related to the intrinsic properties of the components, the substrate properties and the solvent evaporation rate, indicating that with a suitable combination of these factors it can lead to polymeric composite materials with variable structures and properties.

References

1. H. A. Bruck, J. J. Evans and M. L. Peterson, *Exp. Mech.* **42**, 361 (2002).
2. L. L. Hench and J. M. Polak, *Science* **295**, 1014 (2002).

3. T. Akaike, *Biofunctional Materials — Fundamental for Artificial Organs, Tissue Engineering and Regenerative Medicine*. Corona, Tokyo (2005).
4. G. Krausch, E. J. Kramer, M. H. Rafailovich and J. Sokolov, *Appl. Phys. Lett.* **64**, 2655 (1994).
5. O. Ikkala and G. T. Brinke, *Science* **295**, 2407 (2002).
6. S. Amada, Y. Ichikawa, T. Munnekta, T. Munekata, Y. Nagase and H. Shimizu, *Composites* **28B**, 13 (1997).
7. S. Suresh, *Science* **292**, 2447 (2001).
8. K. Suganuma, T. Okamoto, M. Shimada and M. J. Koizumi, *J. Am. Ceram. Soc.* **66**, c117 (1983).
9. T. Ishikawa, H. Yamaoka, Y. Harada, T. Fujii and T. Nagasawa, *Nature* **416**, 64 (2002).
10. P. Czubarow and D. Seyferth, *J. Mater. Sci.* **32**, 2121 (1997).
11. B. Hexig, H. Alata, N. Asakawa and Y. Inoue, *J. Polym. Sci. B: Polym. Phys.* **43**, 368 (2005).
12. B. Hexig, H. Alata and Y. Inoue, *J. Polym. Sci. B: Polym. Phys.* **43**, 3069 (2005).
13. Y. Agari, A. Shimada, A. Ueda and S. Nagai, *Macromol. Chem. Phys.* **197**, 2017 (1996).
14. X. M. Xie, T. J. Xiao, Z. M. Zhang and A. J. Tanioka, *J. Colloid Interface Sci.* **206**, 189 (1998).
15. B. Hexig, H. Alata, N. Asakawa and Y. Inoue, *Adv. Funct. Mater.* **15**, 1630 (2005).
16. Y. Kano, S. Akiyama, H. Sano and H. Yui, *Polym. J.* **29**, 158 (1997).
17. V. Zacchi, C. Soranzo, R. Cortivo, M. Radice, P. Brun and G. Abatangelo, *J. Biomed. Mater. Res.* **40**, 187 (1998).
18. J. Aigner, J. Tegeler, P. Hutzler, D. Campoccia, A. Pavesio, C. Hammer, E. Kastenbauer and A. Naumann, *J. Biomed. Mater. Res.* **42**, 172 (1998).
19. L. A. Solchaga, J. E. Dennis, V. M. Goldberg and A. I. Caplan, *J. Orthop. Res.* **17**, 205 (1999).
20. J. U. Park and T. Tsuchiya, *J. Biomed. Mater. Res.* **60**, 541 (2002).
21. R. Yoshida, K. Uchida, Y. Kaneko, K. Sakai, A. Kikuchi, Y. Sakurai and T. Okano, *Nature* **374**, 240 (1995).
22. N. Yamada, T. Okano, H. Sakai, F. Karikusa, Y. Sawasaki and Y. Sakurai, *Makromol. Chem. Rapid Commun.* **11**, 571 (1990).
23. T. Okano, N. Yamada, H. Sakai and Y. Sakurai, *J. Biomed. Mater. Res.* **27**, 1243 (1993).
24. S. Ohya, H. Sonoda, Y. Nakayama and T. Matsuda, *Biomaterials* **26**, 655 (2005).
25. H. Tan, C. M. Ramirez, N. Miljkovic, H. Li, J. P. Rubin and K. G. Marra, *Biomaterials* **30**, 6844 (2009).
26. J.-P. Chen and T.-H. Cheng, *Polymer* **50**, 107 (2009).
27. J. E. Scott, *Ciba Foundation Symp.* **143**, 6 (1989).
28. J. E. Scott, C. Cummings, A. Brass and Y. Chen, *Biochem. J.* **274**, 699 (1991).

—Article—

ヒト間葉系幹細胞の網羅的遺伝子発現解析 —無血清培地を用いた *in vitro* 培養期間中の遺伝子発現の変化について—

澤田留美,*,[a] 山田貴史,[a] 土屋利江,[b] 松岡厚子[a]

A Microarray Analysis of the Effects of Serum-free Medium on Gene Expression Changes in Human Mesenchymal Stem Cells during the *in Vitro* Culture

Rumi SAWADA,*,[a] Takashi YAMADA,[a] Toshie TSUCHIYA,[b] and Atsuko MATSUOKA[a]

[a]*Division of Medical Devices, National Institute of Health Sciences, 1–18–1 Kamiyoga, Setagaya-ku, Tokyo 158–8501, Japan, and* [b]*Medical Center for Translational Research, Osaka University Hospital, 2–15 Yamadaoka, Suita, Osaka 565–0871, Japan*

(Received June 18, 2010; Accepted July 5, 2010; Published online July 6, 2010)

We examined the effects of serum-free medium on the gene expression changes in human mesenchymal stem cells (hMSCs) during the *in vitro* culture using a DNA microarray analysis. In this study, we cultured hMSCs with two kinds of medium; 1) MSCGM (contain 10% fetal bovine serum) or 2) STK2 (serum-free medium developed for mesechymal stem cells multiplication), and compared hMSCs proliferation, cell morphology, and gene expression changes until 50 days culture. Expression analysis was performed with Affymetrix GeneChip Human Genome U133 Plus 2.0 Array. hMSC proliferation was significantly higher in STK2 medium than in MSCGM medium. The cell morphology of hMSC cultured with STK2 was not significantly changed in 50 days culture. The gene expression changes in hMSCs during the *in vitro* culture were significantly higher in STK2 than in MSCGM. After 50 days culture, 1991 genes were significantly changed the expression levels compared with 3 days in STK2 but not MSCGM. The expressions of genes related to cell cycle, cancer, proliferation, and cell growth were significantly changed by STK2 for 50 days culture. It was also changed by STK2 that the expressions of genes related to the signaling pathways contain various growth factors, such as IGF-1, FGF, TGF-β, EGF, proliferation, and cell cycle. These results suggest that STK2 may be useful to obtain an enough number of hMSC cells for tissue engineered medical devices in short-term, however, it should be recognized that STK2 would alter the expressions of genes related to a variety of signaling pathways in hMSC if the culture period would be extended to obtain a large number of cells.

Key words——human mesenchymal stem cell; gene expression; serum-free medium; proliferation; *in vitro* culture

緒　　言

近年，iPS 細胞樹立の発表が世界的に脚光を浴び，iPS 細胞の再生医療への応用に大きな期待が寄せられている．しかしながら，iPS 細胞は「万能」と呼ばれる多分化能を持つ一方で，組織再生の目的に沿った iPS 細胞の適切な作製法や制御法の確立の必要性，さらにがん化の可能性といった安全性の問題もあり，再生医療への臨床応用や実用化にはまだ少し時間を要するであろう．一方，成体幹細胞の一種である間葉系幹細胞は，骨，軟骨，筋，腱，脂肪，さらには神経細胞や肝細胞，心筋，皮膚など胚葉を越えた分化も報告されており幅広い再生医療分野での利用が期待され，実用化に向けた研究開発が進められている．現在，骨髄，脂肪組織，臍帯血由来の間葉系幹細胞が，その採取技術及び *in vitro* での培養技術も確立されており，細胞組織医療機器の材料として現段階で最も実用に近いものの 1 つであると考えられる．実際に細胞組織医療機器に利用するためには幹細胞を生体内から取り出して *in vitro* で培養して増殖させるという工程を経なければならないため，*in vitro* での培養期間中に幹細胞が目的以外の形質を持った細胞に変化しないことを確認し，患者に戻される細胞の安全性を担保する方法を確立することは大変重要であろう．

in vitro での様々な細胞培養条件は間葉系幹細胞の性質に影響を及ぼすため，本研究では細胞の培養

[a]国立医薬品食品衛生研究所医療機器部，[b]大阪大学医学部附属病院未来医療センター
*e-mail: rsawada@nihs.go.jp

液に着目し *in vitro* 培養による細胞の変化について検討した．間葉系幹細胞の培養には一般的に牛血清又は自家ヒト血清が培地に添加されるが，牛血清使用による病原性ウイルスやプリオンなどの混入の危険性やヒト血清使用のための患者への身体的負担等の回避のために無血清培地を用いる方法も検討されており，間葉系幹細胞の増殖培養に適した無血清培地も研究開発されている．[1,2] そこで本研究では，間葉系幹細胞の増殖培養用に開発された無血清培地を用いて，ヒト骨髄由来間葉系幹細胞（hMSC）を細胞組織医療機器の材料として臨床現場で利用されることを想定した *in vitro* 培養期間（50日以内）を設定して培養し，このような短期間でも培養期間中に細胞に変化が生じるのかどうか調べるために，増殖能，細胞の形態を検討するとともに，網羅的遺伝子発現解析を行い遺伝子発現の変化について検討した．

実 験 方 法

1. 細胞及び培養 ヒト骨髄由来間葉系幹細胞（hMSC）（Lonza Walkersville, Inc.）を，1）Mesenchymal Stem Cell Growth Medium（MSCGM）（Lonza Walkersville, Inc.）：Mesenchymal Stem Cell Basal Medium（MSCBM）に Mesenchymal Cell Growth Supplement（MCGS）を加えた培地（10%牛胎児血清を含む）又は2）STK2（DS ファーマバイオメディカル）：間葉系幹細胞用無血清培地でそれぞれ培養した．無血清培地である STK2 は，間葉系幹細胞の増殖培養用に開発された培地であり，FGF, PDGF などの成長因子が添加されている．培養期間は，実際に細胞組織医療機器の材料として間葉系幹細胞を用いる場合を想定し妥当な培養期間（多少長めに設定し 50 日以内）とした．

2. Total mRNA の調製 培養期間が3日間，20日間，50日間の細胞からそれぞれ RNeasy Mini Kit（QIAGEN）を用いて total RNA を抽出した．

3. 網羅的遺伝子発現解析 2種類の培地（MSCGM 又は STK2）にてそれぞれの期間培養した hMSC から調製した totalRNA を用いて，Affymetrix GeneChip Human Genome U133 Plus 2.0 Array にて mRNA 発現を網羅的に測定した．それぞれ Technical replicate（Duplicate）にて行った．遺伝子発現解析は，GeneSpring GX 7.3.1（Agilent Technologies）を用いて行った．パスウェイ解析は，Ingenuity Pathway Analysis Software（Ingenuity Systems）を用いて行った．

結 果

ヒト骨髄由来間葉系幹細胞（hMSC）を，10%牛胎児血清を含む培地（MSCGM）と無血清培地（STK2）それぞれの培地で培養した際の増殖曲線を Fig. 1 に示す．hMSC の増殖能は STK2 の方が MSCGM に比べて著しく高かった．MSCGM では 50 日間の培養で約 14000 倍の細胞を得られたが，STK2 では 20 日間で得られており，STK2 を用いることにより MSCGM と比較して 30 日間の培養期間短縮が可能であった．

さらに，hMSC の培養 50 日以内の細胞形態の変化についてそれぞれの培地による影響を比較した．Figure 2 に各培養期間の hMSC の位相差顕微鏡像を示す．培養期間 28 日頃までは培養期間及び培地による細胞形態の変化はあまりみられなかった．培養 50 日後の hMSC は，STK2 では培養初期の形態を比較的保っていたが，MSCGM では細胞が少し広がり扁平化しているのが観察された．

次に，hMSC における *in vitro* 培養 50 日以内の遺伝子発現の変化について，MSCGM と STK2 とを比較した．まずは，培養開始時としてそれぞれ培養3日における mRNA 発現レベルを1とし，20日，50日における変化を Fig. 3 に示した．50 日間の培養期間中のそれぞれの遺伝子発現の変化は，STK2 の方が MSCGM よりも非常に大きかった．実際に

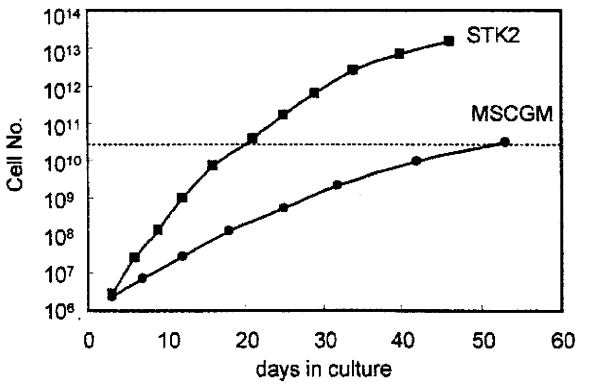

Fig. 1. Proliferation of Human Mesenchymal Stem Cells (hMSCs)

hMSCs were cultured in MSCGM or STK2. They were seeded at a density of 6000 cells/cm^2 and when they were just subconfluent, they were subcultured and the number of cells was counted.

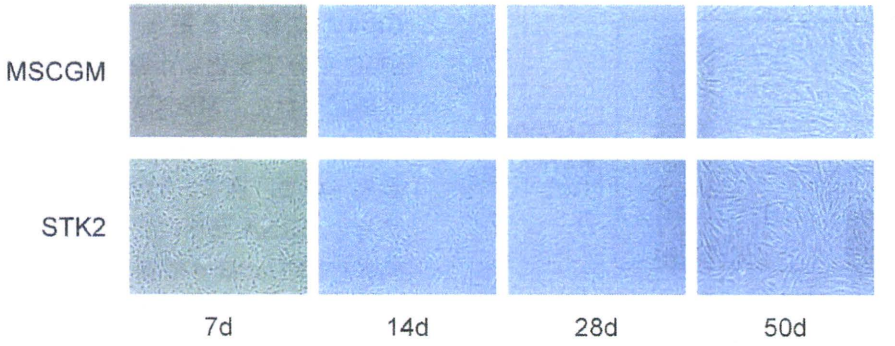

Fig. 2. Cell Morphology of hMSCs Cultured in MSCGM or STK2
They were observed in 7, 14, 28, and 50 days.

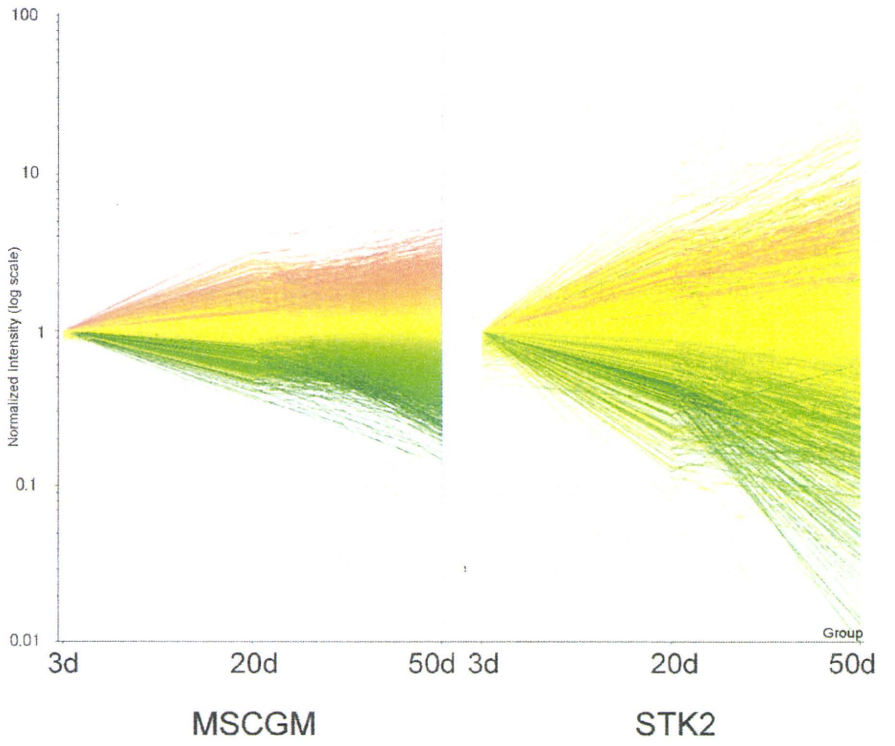

Fig. 3. Changes in Gene Expressions of hMSCs Cultured in MSCGM or STK2 during the *in Vitro* Culture
Each mRNA expression in hMSCs for 3 days culture is expressed as 1, and those for 20 and 50 days are expressed relative to that for 3 days.

培養開始時と比較して有意（2倍以上又は1/2以下）にmRNA発現が変化した遺伝子数をFig. 4に示した．どちらの培地を用いた場合でも，培養開始時と比較して有意にmRNA発現が変化した遺伝子数は培養日数に依存して増加した．hMSC培養20日，50日それぞれにおいて，有意にmRNA発現レベルが変化した遺伝子数はSTK2の方が多く，培養50日では2000以上の遺伝子の発現レベルが培養開始時と比較して有意に変化していた．有意に変化した遺伝子数は，MSCGMでの培養50日とSTK2での培養20日とがほぼ同程度であった．

では，このように*in vitro*培養過程でその発現レベルが変化した遺伝子は，どのような性質（機能）を持つ遺伝子なのだろうか？　変化した遺伝子をそれぞれ抽出してリスト化し，GeneSpring GX 7.3.1にて変化した遺伝子群と同様の機能を持つ遺伝子群を検索することによってhMSCの*in vitro*培養過程でどのような機能を持つ遺伝子群が変化したのか検討した．それぞれの培地で20日及び50日間培養した際に培養開始時と比較して有意に変化した遺伝

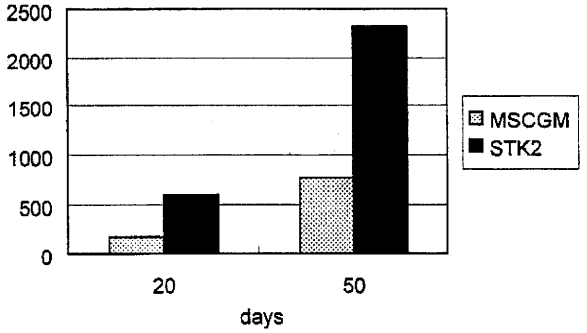

Fig. 4. Number of Genes Whose mRNA Expressions in hMSCs Were Significantly Different from Those for 3 Days Culture

Table 1. The Similar Gene Lists to the Genes Whose mRNA Expressions Significantly Changed during the *in Vitro* Culture of hMSCs

culture period (days)	Media	Number of Genes	Similar List[a]	over lap	*p*-value
20	MSCGM	174	—	—	—
	STK2	603	Cell Cycle	73	5.35E-23
			Cancer	121	5.26E-21
			Proliferation	54	1.08E-08
		(395)	(Cancer)	(69)	(1.38E-08)
			(Proliferation)	(32)	(9.56E-04)
50	MSCGM	762	Cell Cycle	101	8.15E-34
			Proliferation	75	1.01E-14
			Cancer	117	3.57E-11
	STK2	2329	Cancer	318	1.37E-23
			Cell Cycle	152	3.92E-17
			Proliferation	151	2.60E-13
			Cell Growth	40	1.33E-02
		(1991)	(Cancer)	(259)	(4.40E-16)
			(Proliferation)	(116)	(4.52E-07)
			(Cell Cycle)	(94)	(2.90E-03)

[a] The name of lists that resemble the selected list or contain a statistically significant number of overlapping genes. The overlap is calculated using a standard Fisher's exact test and the *p*-value is adjusted with a Bonferroni multiple testing correction.

子数と，それぞれの遺伝子群に有意に重複する遺伝子群を Similar List として Table 1 に示した．（ ）内は，STK2 培養により変化した遺伝子のうち，MSCGM では有意な変化がみられず STK2 でのみ有意な変化がみられた遺伝子について表した．STK2 培養では，20 日の培養から Cell Cycle, Cancer, Proliferation に係わる遺伝子の発現に変化がみられ，50 日では遺伝子数の増加に伴いさらに Cell Growth に係わる遺伝子に変化が認められた．STK2 のみで変化した遺伝子は，50 日では 2000 近く確認された．MSCGM 培養では，50 日間で Cell Cycle, Proliferation, Cancer に係わる遺伝子の変化がみられた．次に，MSCGM では 50 日間の培養中にその mRNA 発現に変化がなかった遺伝子のうち STK2 では *in vitro* 培養により有意に変化した遺伝子群について，どのようなパスウェイに係わる遺伝子が変化しているのか調べた．Ingenuity Pathway Analysis により検討し，Table 2 に上位 20 のパスウェイとそこに含まれる遺伝子を示した．IGF-1, FGF, TGF-β, EGF, HGF, PDGF, MYC, JUN, SMAD3, TP53 等，様々な成長因子や細胞増殖又は細胞周期等に係わる遺伝子の発現が変化しており，多くのシグナル伝達系が STK2 培養によって変化することがわかった．

考　　察

様々な疾病などによる組織や器官の機能不全に対して組織再生又は機能回復を目指した「再生医療」の早期実現が待望されており，現在その材料の 1 つとして間葉系幹細胞の有用性が期待されている．幹細胞の大きな特徴としては，多分化能を保ちつつ増殖能を持つ点であり，実際に再生医療を目的として幹細胞を利用するためには幹細胞を体内から取り出した後，必要細胞数まで *in vitro* で培養して増殖させなければならない．安全性の観点から最も懸念されるのは，*in vitro* 培養中の細胞のがん化である．これまで，脂肪由来[3]又は骨髄由来[4]の間葉系幹細胞を 4,5 ヵ月–2 年といった長期間培養することによって細胞のがん化が起こるという報告がある一方で，骨髄由来[5]でも脂肪由来[6]でも hMSC の長期培養による形質転換はみられないとの報告もなされている．これらの報告の違いは，細胞のドナーの個体差も大きく係わるとも考えられる．実際，hMSC の多くが早いものでは 5 週間程度の培養期間で細胞老化の現象を示す．いずれにしろ，*in vitro* 培養期間が短い方ががん化のような好ましくない変化の可能性をより低減できると考えてよいであろう．そのためには短期でより多くの細胞を得る必要があり，その目的に合った培養条件は重要なポイントである．本研究で用いた無血清培地（STK2）は，牛血清使用による危険性の回避と同時に間葉系幹細胞の